
Inventory of the SI Appendix

- Figure S1. The *fam91a1* MO significantly decreased the mRNA levels of *fam91a1* in zebrafish.
- Figure S2. TBC1D23⁵¹⁴⁻⁵³⁸ directly binds to FAM91A1.
- Figure S3. Electron density map of the TBC1D23 loop with a composite simulated annealing omit map at 2.51 Å resolution and contoured at 1σ
- Figure S4. Sequence comparison of FAM91A1 and TBC1D23 from different model organisms.
- Figure S5. Time-lapse chasing of FAM91A1-GFP and TBC1D23-mCherry colocalization events.
- Figure S6. Endocytosis and intracellular transport of KIAA0319L.
- Figure S7. Knockout of either TBC1D23 or FAM91A1 resulted in abnormal subcellular localization and reduced expression of KIAA0319L in cells.
- Figure S8. TBC1D23 residues that interact with FAM91A1 are required for endosome-to-Golgi trafficking of KIAA0319L.
- Figure S9. TBC1D23 residues interacting with FAM91A1 are required for proper recruitment of CI-MPR and KIAA0319L.
- Table S1. Crystallography Data Collection and Refinement Statistics.
- Table S2. DNA Constructs Used in this Study.
- Table S3. Summary of Antibodies Used in this Study.

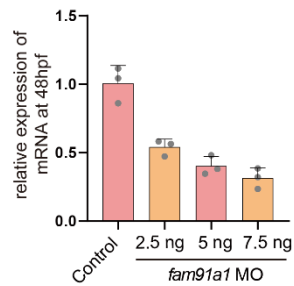


Figure S1. The *fam91a1* MO significantly decreased the mRNA levels of *fam91a1* in zebrafish. qPCR of whole zebrafish tissue extracts shows that *fam91a1* MO effectively reduces *fam91a1* mRNA level. Control: control MO injection; *fam91a1* MO: *fam91a1* MO injection. All injections were performed at the one cellular stage of zebrafish development.

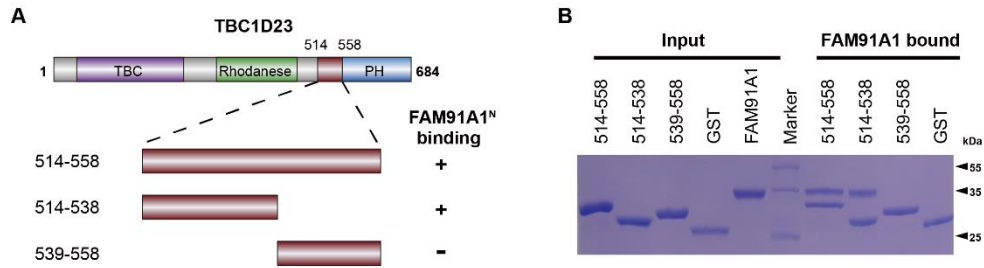


Figure S2. TBC1D23⁵¹⁴⁻⁵³⁸ directly binds to FAM91A1.

(A) Schematic representation of the TBC1D23 fragments used in B. +, indicates that the truncated TBC1D23 is bound to FAM91A1^N (residues 1-328); -, indicates that the truncated TBC1D23 is not bound to FAM91A1^N detected by pulldown.

(B) GST pull-down assays performed with GST–TBC1D23 fragments, or GST, and purified FAM91A1^N (residues 1-328). Shown is the Coomassie blue-stained SDS/PAGE gel of input (left) and bound (right) samples.

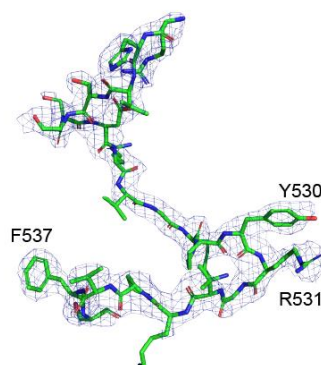


Figure S3. Electron density map of the TBC1D23 loop with a composite simulated annealing omit map at 2.51 Å resolution and contoured at 1σ.

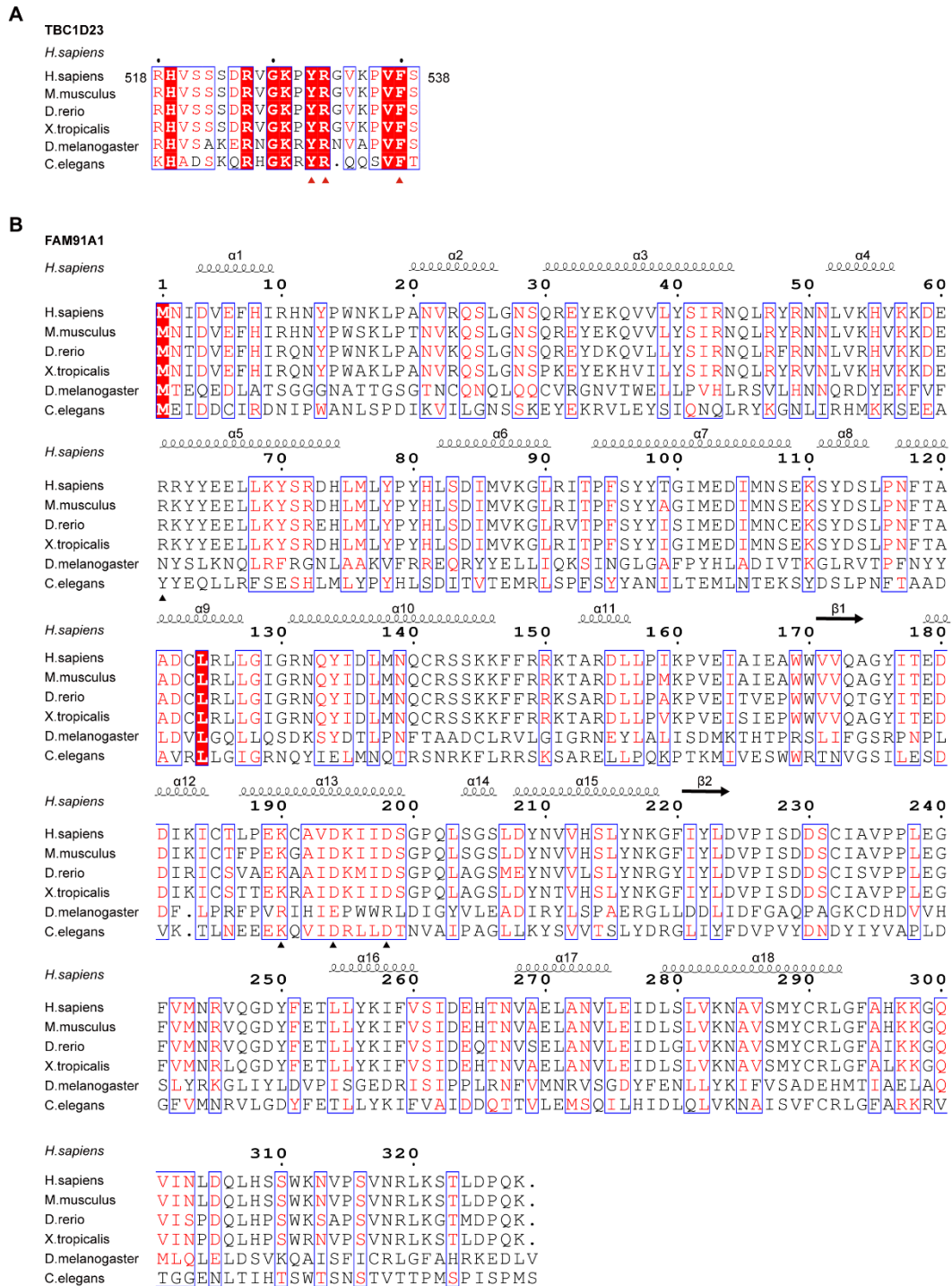


Figure S4. Sequence comparison of FAM91A1 and TBC1D23 from different model organisms.

(A) Sequence comparison of TBC1D23 from different model organisms. The ClustalW tool was used to carry out sequence alignments. Shown is the protein

secondary structure listed (above)and consensus sequence listed (below). ▲ :
FAM91A1-binding site.

(B) Sequence comparison of FAM91A1 from different model organisms. The
ClustalW tool was used to carry out sequence alignments. Shown is the protein
secondary structure listed (above) and consensus sequence listed (below). ▲ :
TBC1D23-binding site.

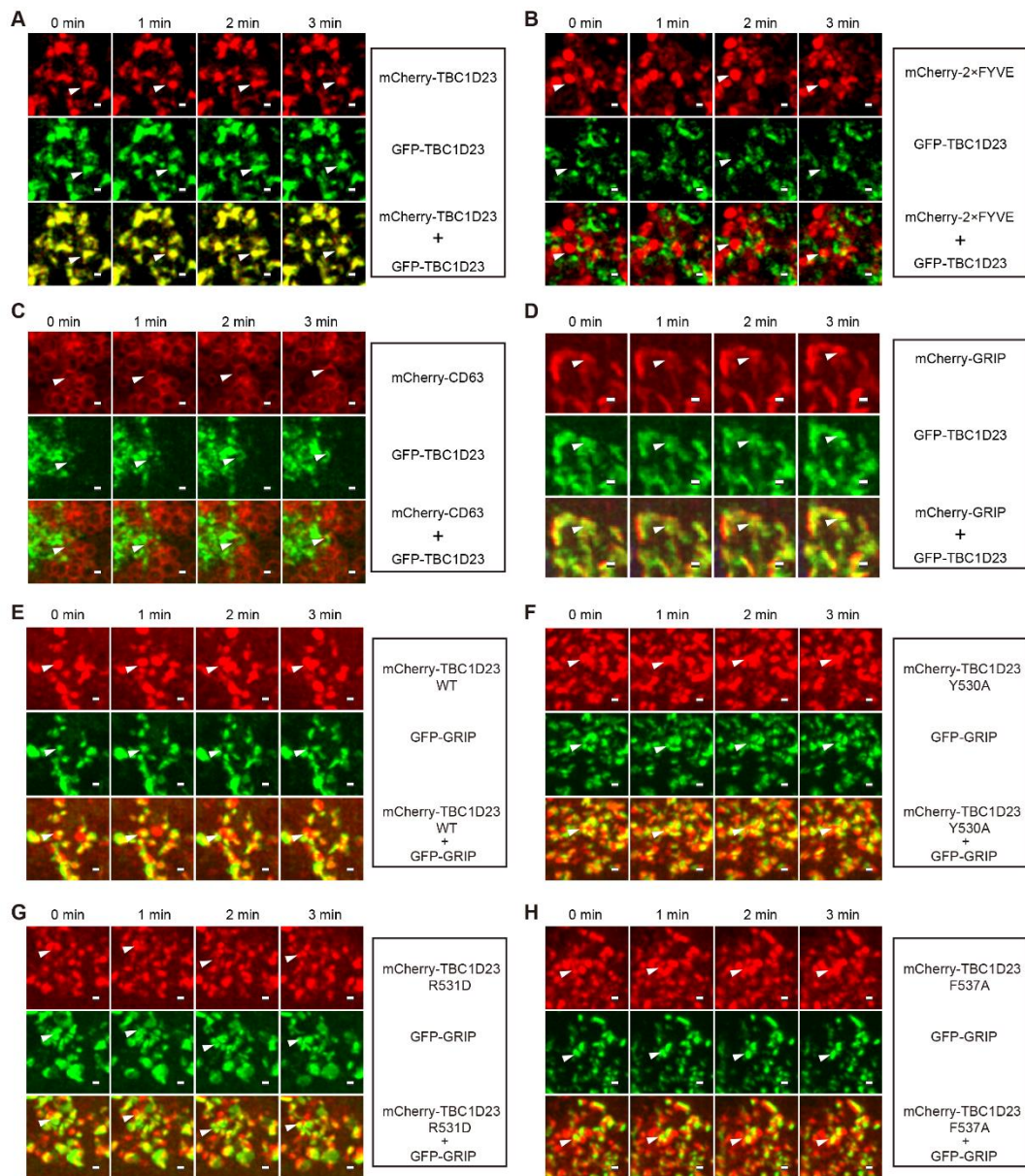


Figure S5. Time-lapse chasing of TBC1D23-GFP and TBC1D23-mCherry colocalization events.

(A) Time-lapse chasing exhibit significant co-localization of TBC1D23-GFP with TBC1D23-mCherry in COS7 cells. The experiment was repeated independently three times. Scale bar: 500 nm.

(B) Time-lapse chasing exhibits negligible co-localization of TBC1D23-GFP with

mCherry-2×FYVE in COS7 cells. The experiment was repeated independently three times. Scale bar: 500 nm. FYVE: the early endosome marker.

(C) Time-lapse chasing exhibit minimal co-localization of TBC1D23-GFP with mCherry-CD63 in COS7 cells. The experiment was repeated independently three times. Scale bar: 500 nm. CD63: the late endosome marker.

(D) Time-lapse chasing exhibit significant co-localization of TBC1D23-GFP with mCherry-GRIP in COS7 cells. The experiment was repeated independently three times. Scale bar: 500 nm. GRIP: the trans-Golgi marker.

(E) Time-lapse chasing exhibit significant co-localization of mCherry-TBC1D23 WT with GFP-GRIP in A549 cells with stably transfected GFP-GRIP. The experiment was repeated independently three times. Scale bar: 1 μm. GRIP: the trans-Golgi marker.

(F) Time-lapse chasing exhibit significant co-localization of mCherry-TBC1D23 Y530A with GFP-GRIP in A549 cells with stably transfected GFP-GRIP. The experiment was repeated independently three times. Scale bar: 1 μm. GRIP: the trans-Golgi marker.

(G) Time-lapse chasing exhibits significant co-localization of mCherry-TBC1D23 R531D with GFP-GRIP in A549 cells with stably transfected GFP-GRIP. The experiment was repeated independently three times. Scale bar: 1 μm. GRIP: the trans-Golgi marker.

(H) Time-lapse chasing exhibits significant co-localization of mCherry-TBC1D23 F537A with GFP-GRIP in A549 cells with stably transfected GFP-GRIP. The

experiment was repeated independently three times. Scale bar: 1 μm . GRIP: the trans-Golgi marker.

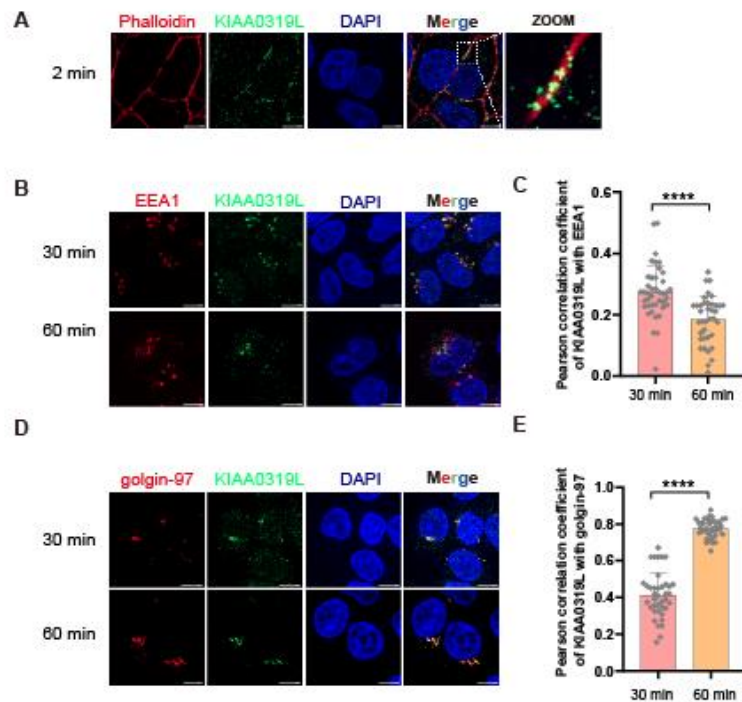


Figure S6. Endocytosis and intracellular transport of KIAA0319L.

(A) HeLa cells were incubated with anti-KIAA0319L antibodies for 1 hour at 4°C, washed, and then transferred to 37°C for 2 minutes to allow internalization. KIAA0319L primarily co-localized with, Phalloidin, a marker for plasma membrane, 2 min after internalization. Scale bar: 10 μ m.

(B) HeLa cells were incubated with anti-KIAA0319L antibodies for 1 hour at 4°C, washed, and then transferred to 37°C for 30 or 60 min. Cells were fixed and stained with antibodies against KIAA0319L or EEA1, a marker for early endosome. Scale bar: 10 μ m.

(C) Colocalization analysis between KIAA0319L and EEA1 in B. Each dot represents Pearson's correlation coefficients from one cell. Data are presented as mean \pm SD, and P values were calculated using unpaired t test. $0.001 < ****P < 0.0001$; figure is

representative of n = 3 independent experiments with similar results.

(D) HeLa cells were incubated with anti-KIAA0319L antibodies for 1 hour at 4°C, washed, and then transferred to 37°C for 30 or 60 min. Cells were fixed and stained with antibodies against KIAA0319L or golgin-97, a marker for TGN. Scale bar: 10 μm.

(E) Colocalization analysis between KIAA0319L and golgin-97 in D. Each dot represents Pearson's correlation coefficients from one cell. Data are presented as mean ± SD, and P values were calculated using unpaired t test. $0.001 < ****P < 0.0001$; figure is representative of n = 3 independent experiments with similar results.

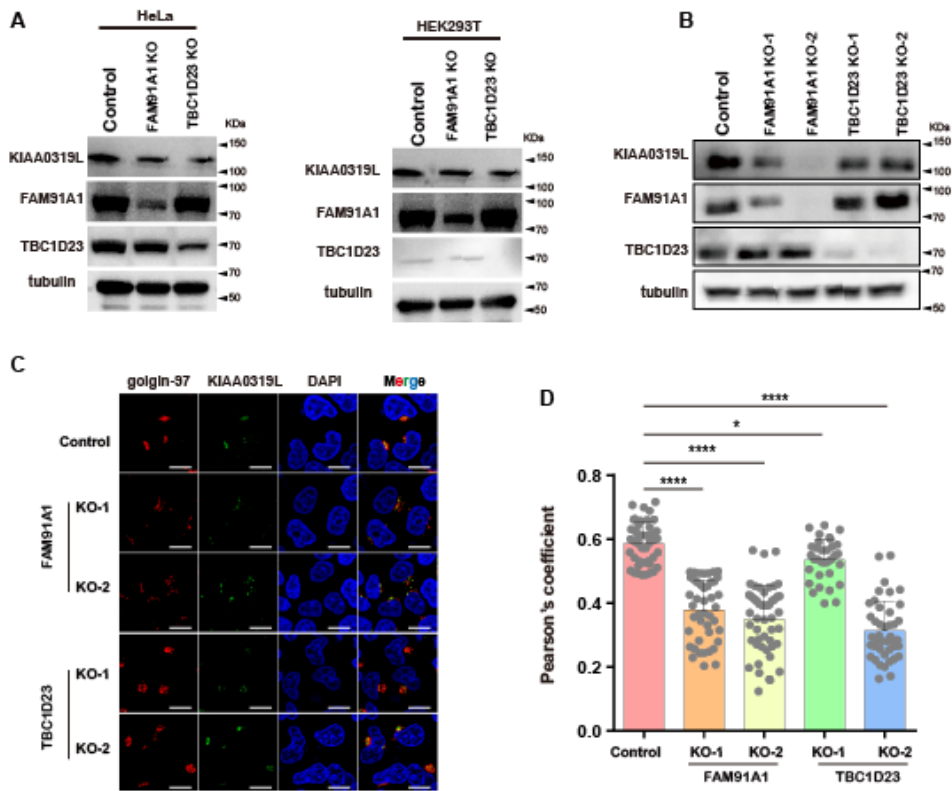


Figure S7. Knockout of either TBC1D23 or FAM91A1 results in abnormal Golgi localization and reduced expression of KIAA0319L in cells.

(A) Depletion efficiency of FAM91A and TBC1D23 in HeLa (left) and 293T cells (right). Tubulin was used as a loading control.

(B) Depletion efficiency of FAM91A and TBC1D23 in monoclonal or polyclonal HeLa cells generated through serial dilution. Tubulin was used as a loading control.

(C) Subcellular location of KIAA0319L in control, FAM91A KO, and TBC1D23 KO HeLa cell lines. Cells were then incubated with antibodies against KIAA0319L (green) and golgin-97 (red). Scale bar: 10 μ m.

(D) Colocalization analysis between KIAA0319L and golgin-97 in C. Each dot represents Pearson's correlation coefficients from one cell. Data are presented as mean

\pm SD, and P values were calculated using one-way ANOVA and Tukey's multiple comparisons test. $*P < 0.05$, $0.001 < ****P < 0.0001$; figure is representative of $n = 3$ independent experiments with similar results.

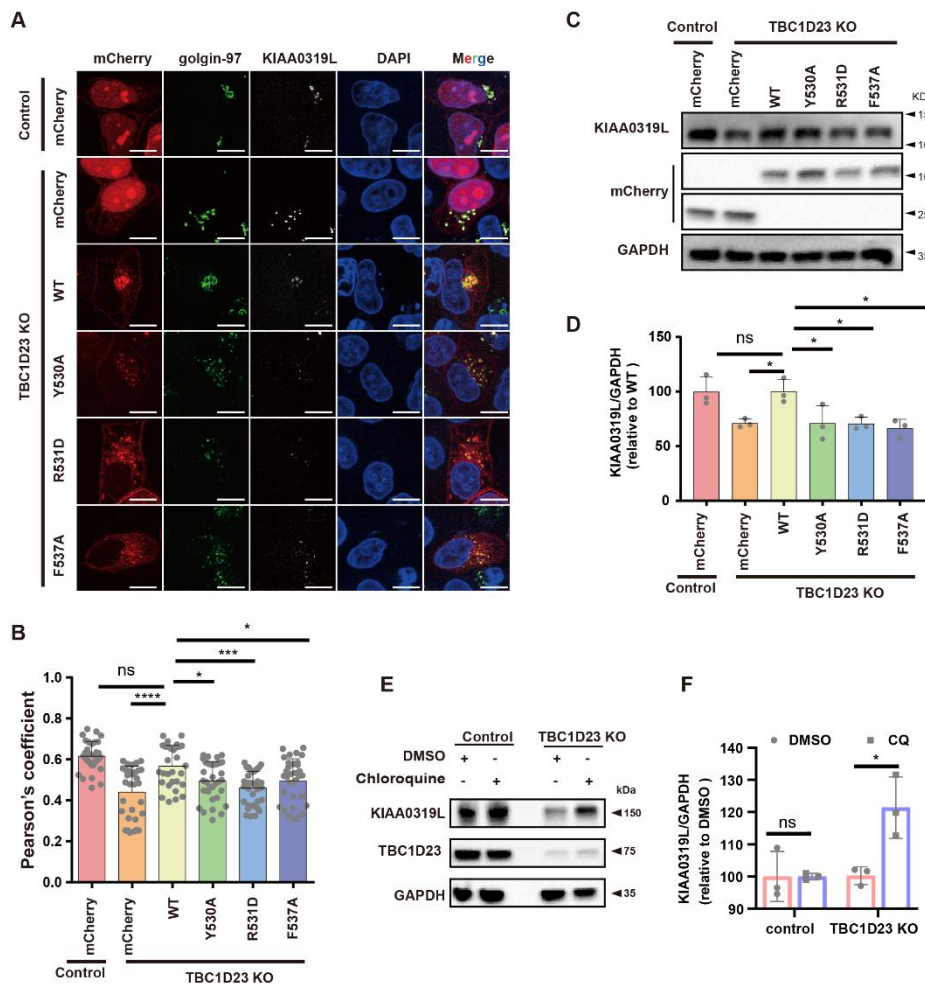


Figure S8. TBC1D23 residues interacting with FAM91A1 are required for endosome-to-TGN trafficking of KIAA0319L

(A) Subcellular location of KIAA0319L in HeLa cell lines. The TBC1D23 KO cells were transiently transfected with mCherry, TBC1D23-mCherry WT, Y530A, R531D, or F537A. Cells were then incubated with antibodies against KIAA0319L (gray) and golgin-97 (green). The cDNA sequence of overexpressed TBC1D23 has been codon-optimized and is not recognized by the gRNA sequences in TBC1D23 knockout cells.

Scale bar: 10µm

(B) Colocalization analysis between KIAA0319L and golgin-97 in A. Each dot

represents Pearson's correlation coefficients from one cell. Data are presented as mean \pm SD, and P values were calculated using one-way ANOVA and Tukey's multiple comparisons test. Ns: not significant, *P < 0.05, 0.001 < ****P < 0.0001; the figure is representative of n = 3 independent experiments with similar results.

(C) Immunoblot of whole-cell extracts showing that knockout of TBC1D23 decreased the total protein level of KIAA0319L. Transient expression of WT, but not these mutants or mCherry, could rescue the reduction partially.

(D) The relative abundance of KIAA0319L compared to GAPDH was quantified in Graph C and compared to the wild-type group. Data are presented as mean \pm SD, and P values were calculated using one-way ANOVA and Tukey's multiple comparisons tests. Ns: not significant, *P < 0.05.

(E) Immunoblotting analysis of whole-cell lysates revealed that knockout of TBC1D23 decreased the total protein level of KIAA0319L. The diminished KIAA0319L resulting from TBC1D23 reduction exhibited partial recovery when exposed to the lysosome inhibiting agent chloroquine.

(F) The relative abundance of KIAA0319L compared to GAPDH was quantified in Graph E and compared to the DMSO-treatment group. Data are presented as mean \pm SD, and P values were calculated using t test. Ns: not significant, *P < 0.05.

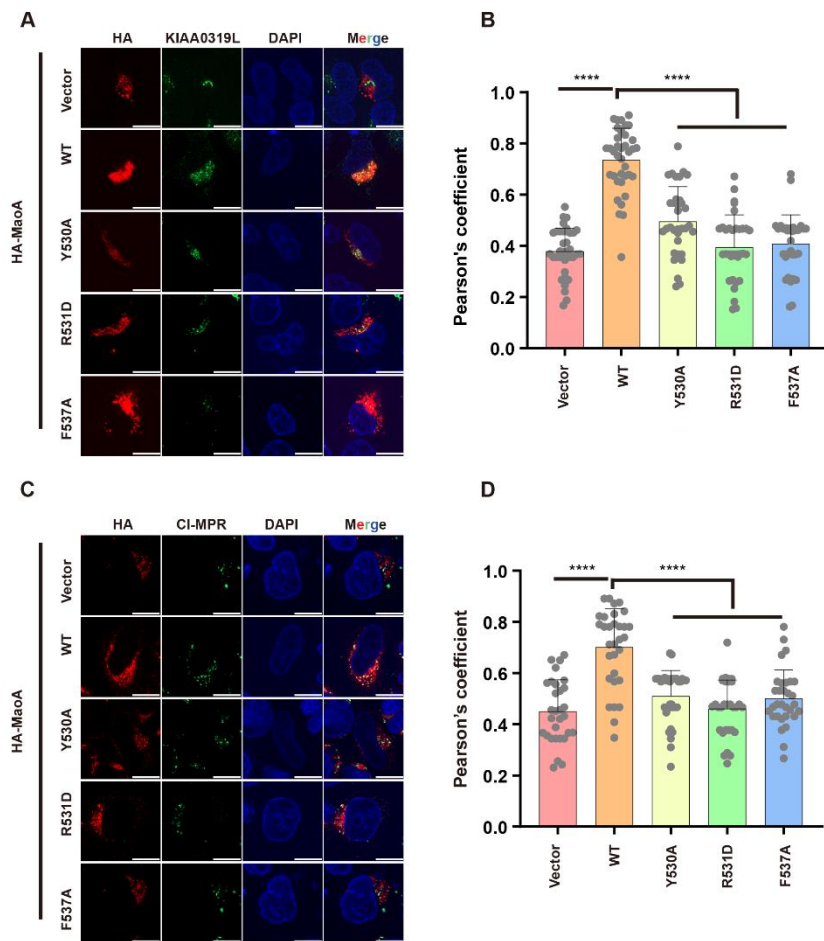


Figure S9. TBC1D23 residues interacting with FAM91A1 are required for proper recruitment of KIAA0319L and CI-MPR.

(A) Mitochondria recruitment assay. Confocal micrographs showing that TBC1D23 WT HA-MaoA, the mutants deficient for FAM91A1 binding (Y530A, R531D, or F537A) or empty vector encoding HA-MaoA, relocates endogenous KIAA0319L to mitochondria in HeLa cells. Scale bar: 10 μ m.

(B) Quantitation of HA colocalization with KIAA0319L in cells in A. Each dot represents Pearson's correlation coefficients from one cell. Data are presented as mean \pm SD, and P values were calculated using one-way ANOVA and Tukey's multiple

comparisons test. $0.001 < ****P < 0.0001$; the figure is representative of $n = 3$ independent experiments with similar results.

(C) Mitochondria recruitment assay. Confocal micrographs showing that TBC1D23 WT HA-MaoA, the mutants deficient for FAM91A1 binding (Y530A, R531D, or F537A) or empty vector encoding HA-MaoA, relocates endogenous CI-MPR to mitochondria in HeLa cells. Scale bar: 10 μm .

(D) Quantitation of HA colocalization with CI-MPR in cells in C. Each dot represents Pearson's correlation coefficients from one cell. Data are presented as mean \pm SD, and P values were calculated using one-way ANOVA and Tukey's multiple comparisons test. $0.001 < ****P < 0.0001$; the figure is representative of $n = 3$ independent experiments with similar results.

Table S1. The x-ray crystallographic data collection and Refinement Statistics.

Dataset	TBC1D23-FAM91A1
Data collection	
Beamline	02U1, SSRF
Wavelength	0.97918
Resolution range*	39.89 - 2.51 (2.6 - 2.51)
Space group	<i>P</i> 21 21 21
Cell dimensions	
a, b, c (Å)	88.2119, 93.5576, 111.514
α , β , γ (°)	90,90,90
Total reflections	64406 (6410)
Unique reflections	32203 (3204)
Multiplicity	2.0 (2.0)
Completeness (%)	99.85% (99.88%)
Dataset	TBC1D23-FAM91A1
Mean I/sigma(I)	12.08 (1.30)
Wilson B-factor	25.83
R-merge	0.02735 (0.4695)
R-meas	0.03868 (0.6639)
R-pim	0.02735 (0.4695)
CC1/2	0.999 (0.666)
Refinement	
Reflections used in refinement	32168 (3204)
Reflections used for R-free	1592 (180)
R-work	0.2531 (0.3149)
R-free	0.2772 (0.3327)
Number of non-hydrogen atoms	5371
Macromolecules	5214
Solvent	157
Protein residues	636

RMS (bonds)	0.016
RMS (angles)	1.85
Ramachandran favored (%)	98.40
Ramachandran allowed (%)	1.60
Ramachandran outliers (%)	0.00
Rotamer outliers (%)	0.86
Clashscore	33.65
Average B-factor	37.76
Macromolecules	37.85
Solvent	34.80

$R_{\text{work}}^{\text{a}} = \sum |F_o - F_c| / |F_o|$, where F_c and F_o are the calculated and observed structure factor amplitudes, respectively $R_{\text{free}}^{\text{b}}$

calculated as for R_{work} but for 5.0% of the total reflections chosen at random and omitted from the refinement for all data sets #

values in the parenthesis is information from highest resolution shell.

Table S2. DNA Constructs Used in this Study.

Construct name	Description	Source or reference
FAM91A1		
TBC1D23514-543-FAM91A11-328	GST-Tev-TBC1D23_514-543-3GGS-FAM91A1_1-328	This study
FAM91A1N	His-sumo-Tev-FAM91A1_1-328	This study
FAM91A1N R61A	His-sumo-Tev-FAM91A1_1-328_R61A	This study
FAM91A1N KDAA	His-sumo-Tev-FAM91A1_1-328_K190A/D194A	This study
FAM91A1N D198R	His-sumo-Tev-FAM91A1_1-328_D198R	This study
FAM91A1-WT	FAM91A1-WT-GFP	This study
FAM91A1- R61A	FAM91A1-R61A-GFP	This study
FAM91A1-KDAA	FAM91A1-KD ^{AA} -GFP	This study
FAM91A1-D198R	FAM91A1-D198R ^A -GFP	This study
TBC1D23		
TBC1D23-514-558	GST-Tev-TBC1D23_514-558	This study
TBC1D23-514-538	GST-Tev-TBC1D23_514-538	This study

TBC1D23-539-558	GST-Tev-TBC1D23_539-558	This study
TBC1D23-514-558_H519W	GST-Tev-TBC1D23_514-558_H519W	This study
TBC1D23-514-558_D524R	GST-Tev-TBC1D23_514-558_D524R	This study
TBC1D23-514-558_Y530A	GST-Tev-TBC1D23_514-558_Y530A	This study
TBC1D23-514-558_R531D	GST-Tev-TBC1D23_514-558_R531D	This study
TBC1D23514-558_F537A	GST-Tev-TBC1D23_514-558_F537A	This study
TBC1D23-514-558_T514A	GST-Tev-TBC1D23_514-558_T514A	This study
TBC1D23-514-558_P529A	GST-Tev-TBC1D23_514-558_P529A	This study
TBC1D23-514-558_V533I	GST-Tev-TBC1D23_514-558_V533I	This study
TBC1D23-514-558_K534N	GST-Tev-TBC1D23_514-558_K534N	This study
TBC1D23-514-558_R531C	GST-Tev-TBC1D23_514-558_R531C	This study

TBC1D23-514-558_R531H	GST-Tev-TBC1D23_514-558_ R531H	This study
TBC1D23-514-558_F537L	GST-Tev-TBC1D23_514-558_ F537L	This study
TBC1D23-WT	TBC1D23-WT-mCherry	(Huang et al., 2019)
TBC1D23-H519W	TBC1D23-H519W-mCherry	This study
TBC1D23-524R	TBC1D23-524R-mCherry	This study
TBC1D23-Y530A	TBC1D23-Y530A-mCherry	This study
TBC1D23-R531D	TBC1D23-R531D-mCherry	This study
TBC1D23-F537A	TBC1D23-F537A-mCherry	This study
TBC1D23-T514A	TBC1D23-T514A-mCherry	This study
TBC1D23-P529A	TBC1D23-P529A-mCherry	This study
TBC1D23-V533I	TBC1D23-V533I-mCherry	This study
TBC1D23-K534N	TBC1D23-K534N-mCherry	This study
TBC1D23-R531C	TBC1D23-R531C-mCherry	This study
TBC1D23-R531H	TBC1D23-R531H-mCherry	This study
TBC1D23-F537L	TBC1D23-F537L-mCherry	This study
others		
pRSV-Rev	pRSV-Rev	(Yong et al., 2021)
pMDLg/pRRE	pMDLg/pRRE	(Yong et al., 2021)

pMD2.G	pMD2.G	(Yong et al., 2021)
mCherry	pmCherry-N1	(Yong et al., 2021)
GFP	pEGFPN1	(Yong et al., 2021)

Table S3. Summary of Antibodies Used in this Study

Antibody	Company	Catalog	Concentration used or dilution fold
FAM91A1	Abcam	ab81618	1:1000 (WB)
WDR11	Abcam	ab93871	1:1000 (WB)
TBC1D23	proteintech	17002-1-AP	1: 1000 (WB)
mCherry	proteintech	26765-1-AP	1:1000 (WB)
golgin-97	proteintech	12640-1-AP	1:200 (I)
GFP	proteintech	50430-2-AP	1:100 (IF)
KIAA0319L	Abcam	ab105385	1:1000 (WB)
GAPDH	proteintech	10494-1-AP	1:2000 (WB)
tubulin	proteintech	proteintech	1:2000 (WB)
goat anti-mouse IgG-HRP	SAB	L3032-2	1:5000 (WB)
Goat anti-rabbit IgG-HRP	SAB	L3012-2	1:5000 (WB)
FITC affini-pure goat anti-mouse IgG	Jackson ImmunoResearch	115-095-003	0.5 µg/ml

Goat anti-Rabbit IgG			
(H+L) Cross-Adsorbed	ThermoFisher		
Secondary Antibody,		A-11010	1:2000
Alexa Fluor 546			
Alexa Fluor 647			
affinipure goat anti-	Jackson		
mouse IgG	ImmunoResearch	115-605-003	0.5 µg/ml
FITC affinipure goat anti-	Jackson		
rabbit IgG	ImmunoResearch	111-545-003	0.5 µg/ml
